INL/CON-10-19134
PREPRINT

A Simplified HTTR Diffusion Theory Benchmark

HTR 2010

Rodolfo M. Ferrer
Abderrafi M. Ougouag
Farzad Rahnema

October 2010

The INL is a
U.S. Department of Energy
National Laboratory
operated by
Battelle Energy Alliance

Proceedings of HTR 2010
Prague, Czech Republic, October 18-20, 2010
Paper 200

A Simplified HTTR Diffusion Theory Benchmark

Rodolfo M. Ferrer, Abderrafi M. Ougouag, Farzad Rahnema [1]
Idaho National Laboratory
2525 North Fremont Avenue, Idaho Falls, ID 83401 USA
phone: +00-1-208-5267659, Rodolfo.Ferrer@inl.gov

[1]*Nuclear and Radiological Engineering and Medical Physics Programs,*
George W. Woodruff School
Georgia Institute of Technology, Atlanta, Georgia, 30332 USA

Abstract –*The Georgia Institute of Technology (GA-Tech) recently developed a transport theory benchmark based closely on the geometry and the features of the HTTR reactor that is operational in Japan. Though simplified, the benchmark retains all the principal physical features of the reactor and thus provides a realistic and challenging test for the codes. The purpose of this paper is twofold. The first goal is an extension of the benchmark to diffusion theory applications by generating the additional data not provided in the GA-Tech prior work. The second goal is to use the benchmark on the HEXPEDITE code available to the INL. The HEXPEDITE code is a Green's function-based neutron diffusion code in 3D hexagonal-z geometry. The results showed that the HEXPEDITE code accurately reproduces the effective multiplication factor of the reference HELIOS solution. A secondary, but no less important, conclusion is that in the testing against actual HTTR data of a full sequence of codes that would include HEXPEDITE, in the apportioning of inevitable discrepancies between experiment and models, the portion of error attributable to HEXPEDITE would be expected to be modest. If large discrepancies are observed, they would have to be explained by errors in the data fed into HEXPEDITE. Results based on a fully realistic model of the HTTR reactor are presented in a companion paper. The suite of codes used in that paper also includes HEXPEDITE. The results shown here should help that effort in the decision making process for refining the modeling steps in the full sequence of codes.*

I. INTRODUCTION

In order to determine the accuracy of various spatial discretization methods for the solution of the neutron diffusion equation, such as the Finite Difference Method (FDM) [1], Finite Element Methods (FEM) [1], and Nodal Methods [2], it is desirable to establish computational benchmarks that approximately represent the salient neutronic features of a certain reactor core design. In particular, the Very High Temperature Reactor (VHTR) [3] represents a unique challenge to current neutronic analysis capabilities due to its optical thickness (or thinness) [4] and spectral interpenetration between the core and reflector regions.

I.A. Motivation

While standard numerical benchmarks for hexagonal-geometry diffusion theory eigenvalue calculations exist, such as those found in the ANL Benchmark Book [5], these have been historically geared toward fast spectrum and VVER reactor physics. For example, the majority of previous hexagonal geometry diffusion theory numerical benchmarks tended to define energy group boundaries such that the resulting scattering matrix only exhibits downscattering. Clearly, this is not sufficient to capture the neutronic features of a graphite-moderated High Temperature Reactor (HTR), such as the prismatic VHTR.

The motivation for proposing this Simplified HTTR Diffusion Theory benchmark is to provide methods developers with simple model that exhibits all the major neutronic features of the prismatic VHTR, while retaining the simplicity expected in a numerical benchmark.

I.B. Previous Work

Previous work in the area of numerical benchmark preparation has been performed by Z. Zhang, F. Rahnema, et al [6], which culminated in the publication of a simplified two-dimensional HTTR benchmark problem geared toward transport theory-based solution algorithm. While this particular benchmark does not exclude the traditional homogenization paradigm, based on transport theory-based lattice calculations coupled with subsequent nodal diffusion solutions, it is advantageous in our view to produce a diffusion theory benchmark based on a single homogenizations approach, hence circumventing the difficulty presented by comparing nodal diffusion solutions based on different cross-section generation procedures.

I.C. Scope of Work

The starting point of the simplified HTTR benchmark was the experimental High Temperature Engineering Test Reactor (HTTR) [7]. The HTTR is a graphite-moderated, high-temperature, gas-cooled prismatic reactor which shares many of the same design features as the prismatic VHTR, such as helium coolant and graphite blocks which serve as the moderator, reflector, and structural material. In addition, fuel pins consist of fuel compacts which are composed of coated UO_2 fuel particles and graphite matrix. In order to create a *simplified* numerical benchmark, certain geometric and compositional features were eliminated or homogenized, which did not contribute to the fundamental physics of the reactor core. Finally, three configurations were generated in the benchmark preparation: all control rods inserted, some control rods withdrawn, and all control rods withdrawn.

In order to generate a simplified HTTR diffusion theory benchmark, our starting point was the simplified HTTR benchmark described above. The set of reference, multi-group, multi-region transport cross-sections were used to solve the transport equation at the full-core level with full geometric detail, hence obtaining a suitable flux solution for subsequent homogenization. The adequacy of the transport solution was assessed by comparing the resulting multiplication factors and fuel block-averaged pin fission distributions for all three HTTR configurations against the reference multi-group Monte Carlo solutions [6].

In order to generate the multi-group diffusion theory data, certain simplifying assumption had to be introduced in order to make the benchmark useful. Since the flux solution will be different at different locations over the core (even over regions with identical material compositions), it is possible to generate multi-group diffusion theory data for each individual fuel block. Clearly this would complicate the benchmark data in such a way as to make it unsuitable for general use. Hence an identical scheme as the one used in the simplified HTTR benchmark was applied in which the multi-group cross-section data are averaged or homogenized over multiple blocks. Additional assumptions are discussed in later in this article.

In order to obtain a reference solution for this diffusion benchmark, a set of fine-mesh FDM computations were performed which yielded high-accuracy estimates for the multiplication factor and region-averaged, group-dependent, normalized flux values. These reference values are used to compare against highly-efficient results from two nodal approaches: the Nodal Green's Function Method (NGFM), and the Nodal Expansion Method (NEM). In addition, a comparison of the FDM solution to the Nodal Transport (NT) results is performed for completeness.

II. THE HTTR PHYSICS CONFIGURATION

The original HTTR start-up benchmark [7] provided detailed geometric, compositional, and measurement data for the validation of neutronic analysis computational methods. While useful for the purposes of validating computer codes, the discrepancy associated with homogenization and truncation error in the deterministic transport and diffusion theory solvers were difficult to assess, given the uncertainties in cross-section and compositions present in the HTTR. This is evidenced by the significant discrepancy between measured criticality and *a posteriori* Monte Carlo results [8]. Hence, there is a need to obtain numerical benchmarks in which material and cross-section differences (and uncertainties) can be set aside and the adequacy of deterministic solvers assessed.

II.A. The Simplified HTTR Transport Theory Benchmark

In order to simplify the HTTR geometry, certain geometry and composition details were neglected and/or homogenized. The compositions and impurities of graphite were simplified to two typical values, instead of ten as-built values. Certain geometric details, such as gaps between blocks, plugs in fuel holes, handling holes in block, neutron shielding pins in the bottom, etc. were neglected. The composition (boron enrichment) on the burnable poisons (BPs) within a fuel block was averaged into a single concentration over all three BPs. In addition, the number of control rod (CR) holes per control block was reduced from three to a single, symmetric CR hole. Material compositions were homogenized axially, thus yielding a two-dimensional benchmark with four enrichment zones. Finally, the domain shape of the HTTR was changed from a 'jagged' edge, into a flat-sided outer edge by

splitting the reflector hexagonal shape at the outer boundary of the domain.

Finally, given the presence of coated particles within the fuel compact, some type of double heterogeneity (DH) treatment would have to be implemented in order to take into account the self-shielding effects. For simplicity's sake this effect is neglected and the coated fuel particles and graphite matrix were homogenized into a single material.

Once these simplifications were introduced, a set of HELIOS calculations were performed at the lattice level (single block for the fuel regions and multi-block for CR and reflector regions) and a six-energy group cross-section data were generated. These data include four unique macroscopic cross-section sets for each of the four fuel pin enrichments. In addition, four cross-section sets were generated for the graphite in the fuel block, CR block, replaceable and permanent reflector. Two sets of cross-section data were also generated for the BP and CR regions.

Given the geometric and material cross-section data described above, three unique configurations for the HTTR were modeled and solved via the multi-group Monte Carlo approach. The three configurations correspond to all control rods inserted (ARI), some control rods withdrawn or partial inserted (PI), and all control rods withdrawn or 'out' (ARO). High-accuracy Monte Carlo solutions were generated based on effective multiplication factor and detailed fuel compact normalized fission density distributions, along with normalized absorption rates for burnable poisons and CRs.

II.B. HELIOS-2 Modeling

In order to generate a simplified HTTR diffusion theory solution, it was necessary to obtain an accurate solution for the scalar flux. Numerous transport solvers based on deterministic methods were evaluated for this task. The HELIOS [9] lattice physics code was selected due to its geometric flexibility and the availability for two standard transport discretizations: the Collision Probability (CP) method and the Method of Characteristics (MOC). In the current work both methods are exercised and compared against the reference solution.

The initial metric used to determine the adequacy of the deterministic method (and associated spatial mesh) involved the comparison between the HELIOS and multi-group Monte Carlo solution. The second metric used in comparing the two solutions is based on the percentage error in the block-averaged normalized fuel pin fission densities. These serve as a necessary, but perhaps not always sufficient, measure of the adequacy of the deterministic solution.

Before modeling the entire full-core HTTR benchmark geometry, a set of parametric studies was performed in order to determine the adequate spatial mesh. Once the benchmark macroscopic cross-section libraries for HELIOS were processed, simple fuel cell and fuel block models were prepared and compared against the same set of cross-section using multi-group MCNP [10]. The results from these studies not only allow the determination of an adequate spatial mesh, but also verify the correctness of the cross-section libraries.

A set of simplified fuel cells (compact with fuel zone 1 composition plus graphite) were constructed in order to test the convergence of the HELIOS solution and to test the cross-section library. The spatial mesh refinement was based on increasing the number of radial and azimuthal zones. Radial zones correspond to the number of concentric annuli within a pin system, while azimuthal zones split each radial zone into various regions. Figure 1 shows a schematic of the hexagonal fuel cell with increasing azimuthal zones 1 through 5 (azimuthal zones 2 through 5 generate multiples 6). A complementary schematic is shown in Figure 2 which shows the hexagonal fuel cells with increasing radial zones. Note that the fuel zone is shown in blue and graphite in green. Also note that the number of 'flat-source' zones increases with the addition of radial and azimuthal segmentation.

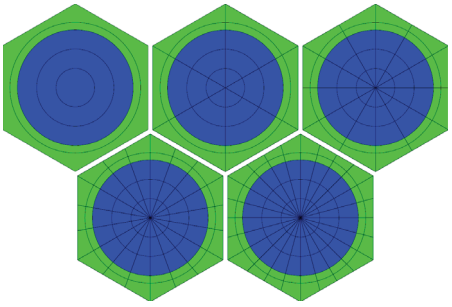

Fig. 1: Fuel cell of simplified HTTR benchmark with increasing azimuthal zones and fixed (three) radial zones shown from top left to bottom right.

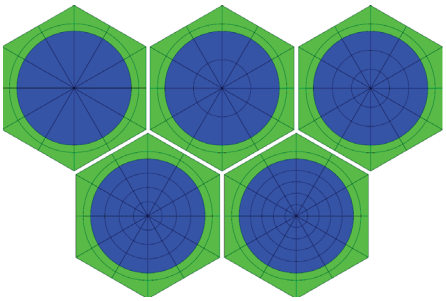

Fig. 2: Fuel cell of simplified HTTR benchmark with increasing radial zones and fixed (twelve) azimuthal zones shown from top left to bottom right.

Reflective boundary conditions were applied to the fuel cell problem and the resulting multiplication factor ($k_{\inf}$) was compared against a high resolution multi-group MCNP estimate of $k_{\inf} = 1.15544(\pm 0.00002)$. In summary, the results

from the set of HELIOS calculations showed that the multiplication factor converges to $k_{\inf} = 1.15544$ once at least four azimuthal and four radial zones are modeled in both CP and MOC options.

In addition to the fuel cell model, an analogous set of fuel block HELIOS models were generated in order to further test the correctness of the benchmark cross-section library and test the spatial mesh. A schematic of the fuel block with the finest spatial grid is shown in Figure 3.

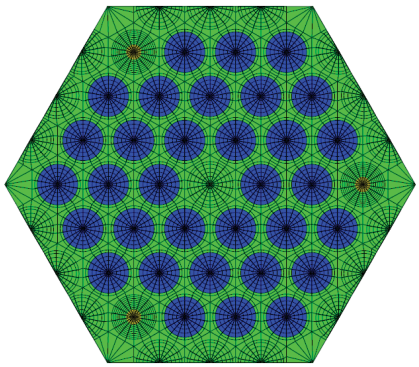

Fig. 3: Fuel block with fuel type 1 enriched compacts (blue) and burnable poisons (yellow) of simplified HTTR benchmark with four azimuthal and five radial zones.

Numerical results showed that at least four azimuthal and five radial zones are required to obtain an adequate solution with respect to the multi-group MCNP result ($k_{\inf} = 1.06293(\pm 0.00005)$). This conclusion is consistent with the numerical experiments performed at the fuel cell level. The burnable poison regions require a finer spatial mesh due to the strong absorption; hence extra radial zones were incorporated into the BP cell. The HELIOS results using the CP option yields $k_{\inf} = 1.06237$, which is $-52.7\,pcm(\Delta k / k)$ lower than the reference MCNP solution. In addition, the HELIOS results using the MOC option yields $k_{\inf} = 1.06278$, which is $-14.1\,pcm(\Delta k / k)$ lower than the reference MCNP solution. Note that both of these calculations use partial coupling, instead of full coupling, hence even with a spatially converged mesh, there are differences between the reference solution and the HELIOS results.

Based on these results, full-core HELIOS models for all three simplified HTTR configurations were created and compared against the reference MCNP results. A schematic of the detailed spatial mesh for the ARI case is shown in Figure 4 below.

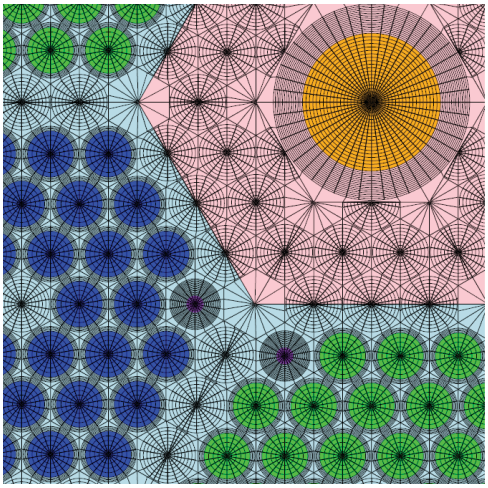

Fig. 4: HELIOS spatial grid for simplified HTTR numerical benchmark with inserted control rod (orange) surrounded by fuel blocks with enrichment types 1 (blue) and 2 (green).

A comparison of the effective multiplication factor between the HELIOS results and the multi-group MCNP reference values is provided in Table 1. The CP and MOC solutions, based on the eigenvalue estimates, show that the MOC results tend to overestimate the eigenvalue with respect to the multi-group MCNP. However, the error in terms of $pcm(\Delta k / k)$ show a better agreement for the ARI and ARO cases between MOC and MCNP as compared to the CP solution and MCNP. In the case of the PI configuration, the results obtained via the CP solution appear to be extremely accurate with respect to the reference solution. Similar grids were used in all three configurations for each CP and MOC option. In fact, the CP and MOC options each use identical spatial mesh for each configuration.

Case	ARI	PI	ARO
HELIOS (CP)	0.89543	1.00394	1.08922
Error (pcm)	-89.3	3.0	-169.6
HELIOS (MOC)	0.89666	1.00451	1.09151
Error (pcm)	48.0	59.8	40.3
Ref. (MCNP)	0.89623	1.00391	1.09107

Table 1: Comparison of HELIOS eigenvalue results for Simplified HTTR Numerical Benchmark to reference multi-group MCNP.

In order to further investigate and verify both HELIOS solutions with respect to the reference MCNP calculation, a comparison of the normalized fission distribution averaged over each fuel block fuel compact was performed for all three cases. A comparison of these fission distributions for ARI case reveals very close agreement between the CP and MOC option. The maximum percent error for

the normalized fission distribution is -1.17% for CP and -1.16% for MOC with respect to MCNP. Both of these maximum errors occur at fuel block type 1 (see Figure 5). For the case involving the PI configuration, an analogous comparison was performed and revealed that the maximum percent error in normalized fission distribution is smaller in the case of CP (-0.42%) and in the case of MOC (-0.93%) with respect to the reference MCNP. In addition, the maximum error in normalized fission distribution also occurs across fuel block type 1. Finally, a comparison of the normalized fission distribution for the ARO configuration revealed a maximum percent error of -1.22% and -0.13% for the CP and MOC solutions with respect to the reference solution, respectively. The location of the maximum error for the CP solution in the case of the ARO configuration is fuel block type 1, whereas the location of the maximum error in the case of the MOC solution has moved to fuel block of enrichment type 2 (see Figure 5).

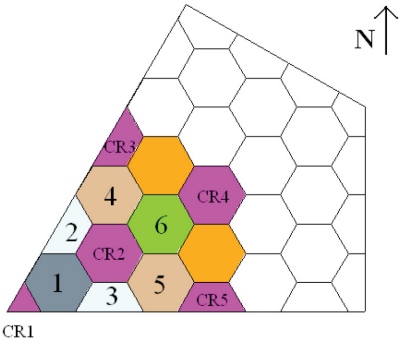

Fig. 5: Schematic of Simplified HTTR Numerical benchmark core geometry (borrowed from [6]).

To further evaluate and interpret these results, a comparison of the normalized absorption rate per control rod region was performed and compared to the reference MCNP solution. A comparison of the percent error in normalized absorption rate for the ARI case reveals a maximum error of -1.44% and -1.38% for the CP and MOC solutions, respectively. Both of these maximum errors occur at the central control rod location, which is located at the hexagonal fuel block on the very center of the active core. A similar pattern was revealed when comparing normalized absorption rates for the PI configuration. The maximum percent error occurs at the center CR location and has a maximum value of -0.75% and -1.45% for the CP and MOC solution, respectively. The lower error in normalized absorption rate and fission distribution (see previous paragraph for discussion) in the CP solution for the PI configuration confirms the rather low error in the CP eigenvalue result. Finally, no comparison is performed of the normalized absorption rate for the ARO configuration, since there are not CRs inserted into the reactor core.

Given the results discussed thus far, the MOC-based HELIOS solutions for the criticality problem seem to be, on average and with respect to the reference MCNP, more accurate than those from CP. It appears that the CP solution is more accurate than the MOC for the PI configuration. However, we feel that using a consistent solution methodology to generate the diffusion benchmark is more important than 'cherry-picking' the best answer.

In order to finalize the transport-based solution of the simplified HTTR benchmark, a set of HELIOS MOC calculations were performed in order to determine the effects of modeling the 'jagged' or corrugated edge of the outer reflector. The modeling approximation avoids the fact that most hexagonal geometry nodal diffusion solvers do not treat re-entrant outer boundaries. However, the explicit modeling of the 'jagged' or corrugated boundary with black boundary conditions will guarantee that there is no re-entrance of the angular flux. In other words, unless the vacuum is explicitly treated between the outer row hexagonal blocks, the HELIOS calculation will assume that this outer edged is 'black', and hence has no incoming angular fluxes.

A comparison of the eigenvalue results generated by the 'original' and 'corrugated' HELIOS models based on the MOC solver for all three configurations is shown in Table 2. This comparison reveals that cases in which the control rods are inserted at the periphery of the reactor (ARI and PI), the effects of the reflector block modeling are roughly $89\,pcm(\Delta k/k)$ in additional reactivity. However, as the case where all the control rods are withdrawn (ARO) shows, the addition of the reflector material may increase the eigenvalue by as much as $265\,pcm(\Delta k/k)$. Due to the optical thinness of graphite-moderated HTRs, the addition of extra reflector material at the periphery of the reactor still affects the fundamental eigenmode, and hence increases the reactivity by reducing the overall leakage of the critical system. The rather significant effects for the ARO case is due to the fact that the highest relative fission distribution is being produced by the fuel assemblies at the periphery of the core (see Table 3 below). In fact, a comparison of the normalized fission distribution over all six fuel blocks for the ARO case reveals that the addition of the reflector material at the periphery of the reflector not only adds excess reactivity to the critical configuration, but slightly increases the normalized power produced by the fuel blocks located in the periphery of the reactor core, while reducing the power produced by the fuel blocks near the center of the core (see Table 3 below).

Case	ARI	PI	ARO
Original	0.89666	1.00451	1.09151

Corrugated	0.89746	1.00540	1.09440
Diff. (pcm)	89.2	88.6	264.8

Table 2: Comparison of HELIOS MOC eigenvalue results for all three HTTR configurations using different outer reflector row modeling.

Fuel Block	Corrugated	Original	Percentage
1	0.95766	0.96006	-0.25%
2	1.00984	1.01205	-0.22%
3	1.01084	1.01315	-0.23%
4	1.00289	1.00200	0.09%
5	1.00468	1.00394	0.07%
6	1.02445	1.02138	0.30%

Table 3: Comparison of normalized fission distribution between 'original' and 'corrugated' reflector models (percentage difference with respect to original model).

The verification of the HELIOS model, based on a comparison to the reference numerical solutions, may now allow the use of the MOC-based flux for spatial homogenization. In particular, we use the MOC-based HELIOS scalar flux to perform flux-weighted homogenization over fuel blocks based on the 'corrugated' model, hence allowing us to quantify the difference between the heterogeneous transport solution and the homogenized 'nodal' model.

II.C. The Simplified HTTR Diffusion Theory Benchmark

The scalar flux solution described thus far is used to generate homogenized cross-section over multiple fuel blocks. However, in order to make the diffusion benchmark as simple as possible, certain approximations had to be made in order to reduce the total number of cross-section regions. Specifically, the flux over all the reflector blocks was spatially homogenized (or averaged) into a single cross-section set. Each material region was used to define each cross-section following the schematic shown in Figure 5. Hence, four unique fuel block materials were defined, along with an inserted CR, a withdrawn CR, a removable reflector, and a permanent reflector material region.

A second approximation involves the definition of the diffusion coefficient. This definition is not unique, as shown in [11], and may indeed affect the accuracy of the nodal diffusion solution. The traditional definition of the diffusion coefficient, based on the P-1 approximation, is used by HELIOS to generate homogenized data and hence it is by default used in this work.

Finally, it is important to recall that improvements upon the nodal 'equivalent' model exist, such as Response Functions (RF) [12], Generlized Equivalence Theory (GET) [13], superhomogenisation (SPH) [14], etc. However, for simplicity, we assume that the set of cross-sections generated in this work are sufficient to compare the efficiency and accuracy of multiple nodal solvers using basic input data.

III. APPLICATION OF NUMERICAL BENCHMARK

A set of tabulated nodal diffusion data for each Simplified HTTR Diffusion Benchmark configuration (ARI, PI, ARO) is included in the Appendix. In order to test the cross-section data itself and compare the differences between the heterogeneous transport reference solution and reference homogenized nodal model, a set of fine-mesh Finite Difference Method (FDM)-based calculations were performed and compared to the MOC results. In addition, a set of computations are also presented in which we compare the heterogeneous transport solution to a Nodal Transport solution. Once these differences are quantified, a comparison of the Nodal Expansion Method (NEM) and the Nodal Green's Function Method (NGFM) in hexagonal geometry is performed with respect to the reference diffusion solution.

III.A. Fine-Mesh Finite Difference Method Reference Solution

In order to determine the accuracy of the spatial homogenization scheme (flux-weighted homogenization) and the low-order diffusion operator approach to the homogenized model, the set of macroscopic cross-sections produced by HELIOS were used by the DIF3D [15] FDM solver to perform eigenvalue-search calculations for all three HTTR configurations. In addition, the VARIANT [16] option present in DIF3D was tested and compared to the reference heterogeneous transport solution. A summary of the results and a comparison of the resulting eigenvalues is shown in Table 4 through 6 below.

Code	Method	k-eff
DIF3D	Fine Mesh FD	0.88802
	Error (pcm)	-1051.7
DIF3D	VARIANT	0.88765
	Error (pcm)	-1092.8
HELIOS	MOC	0.89746

Table 4: Comparison of eigenvalue results for ARI case between reference heterogeneous transport (MOC) and reference homogenized fine-mesh FDM (Diffusion Theory) and high-order homogenized VARIANT.

Code	Method	k-eff
DIF3D	Fine Mesh FD	1.00385

	Error (pcm)	-154.1
DIF3D	VARIANT	1.00336
	Error (pcm)	-202.8
HELIOS	MOC	1.00540

Table 5: Comparison of eigenvalue results for PI case between reference heterogeneous transport (MOC) and reference homogenized fine-mesh FDM (Diffusion Theory) and high-order homogenized VARIANT.

Code	Method	k-eff
DIF3D	Fine Mesh FD	1.09798
	Error (pcm)	326.7
DIF3D	VARIANT	1.09731
	Error (pcm)	265.4
HELIOS	MOC	1.09440

Table 6: Comparison of eigenvalue results for ARO case between reference heterogeneous transport (MOC) and reference homogenized fine-mesh FDM (Diffusion Theory) and high-order homogenized VARIANT.

The set of results obtained via the FDM option (Diffusion Theory) use 21 triangles per hexagonal node, whereas the VARIANT results use a sixth-order spatial polynomial and a P_7 angular expansion. In addition, there is no anisotropic scattering being used for the VARIANT calculation. While this could introduce further differences, highly anisotropic scattering is more characteristic of neutron collisions with heavy nuclides in the fast energy range, such as in a fast reactor.

A comparison of the resulting eigenvalues for the ARI case (Table 4) reveals that both FDM (Diffusion Theory) and VARIANT fail to recover the heterogeneous transport solution by over one thousand pcm. However, a glance at the resulting eigenvalues for the PI and ARO cases (Tables 5 and 6) reveal that this large discrepancy is not present in these cases. Hence, the simple flux-weighted homogenization approach fails to properly account for the absorption occurring within the CR blocks. This observation is supported by the fact that both computations are 'reference' calculations (little truncation error) and each presents a highly-accurate solution for the low-order (Diffusion Theory) and high-order (Transport Theory) operator over the homogenized model. Tables 7 and 8 show the normalized fission. These percentage errors are rather small, particularly if we recall the differences observed between HELIOS MOC and the reference Monte Carlo solution.

Fuel Block	DIF3D (FDM)	HELIOS	Error %
1	1.02446	1.00933	1.50%
2	1.05819	1.05144	0.64%
3	0.97798	0.98452	-0.66%
4	0.96139	0.97019	-0.91%

Table 7: Comparison of normalized fission distributions between heterogeneous transport solution (HELIOS) and homogeneous diffusion solution (DIF3D) for fuel block types 1 through 4 (ARI configuration).

Fuel Block	VARIANT	HELIOS	Error %
1	1.02411	1.00933	1.46%
2	1.05824	1.05144	0.65%
3	0.97822	0.98452	-0.64%
4	0.96120	0.97019	-0.93%

Table 8: Comparison of normalized fission distributions between heterogeneous transport solution (HELIOS) and homogeneous transport solution (VARIANT) for fuel block types 1 through 4 (ARI configuration).

However, a closer look at the homogeneous diffusion and transport solutions reveal that the 'homogenized' solutions over-predict the normalized absorption rate by 6.26 % and 6.18 %, respectively. This results in the overestimation of the absorption across the CR blocks, hence the eigenvalue results are significantly under-predicting the correct reference value. In turn, these results point to the need for more advanced methods that can improve the recovery of heterogeneous transport-based reaction rates across non-multiplying media, such as the Response Function method [12].

Finally, a comparison between the FDM and VARIANT solutions is necessary in order to assess potential transport effects occurring at the 'homogenized model' level. The results for the ARI case are shown in Tables 9 and 10 below. A comparison between the region-averaged fluxes over all six energy groups revealed that differences as larger as -6.93 % may be observed for fast-energy groups at the periphery of the domain (permanent reflector region). Conversely, the difference between the diffusion and transport solution for the homogenized problem is very small across fuel block types 1 through 4. However, the differences begin to increase as we move away from the fuel region and enter the reflector region. Note that these differences are also energy-dependent. The largest errors occur at the fast-energy range (energy groups 1 and 2), whereas differences in the thermal energy groups are minimal across the totality of the reactor core.

Reg.	Group 1	Group 2	Group 3
F1	-0.56%	-0.32%	-0.15%
F2	-0.64%	-0.38%	-0.20%
F3	-0.93%	-0.56%	-0.32%
F4	-1.30%	-0.78%	-0.42%
C1	2.72%	1.11%	0.51%

C2	2.09%	0.76%	0.39%
RR	2.26%	0.94%	0.45%
PR	-6.93%	-2.39%	-0.77%

Table 9: Region-dependent percentage difference between 'fast group' average fluxes from homogenized diffusion (FDM) and transport (VARIANT) results for ARI HTTR configuration.

Reg.	Group 4	Group 5	Group 6
F1	-0.06%	0.03%	0.10%
F2	-0.10%	0.00%	0.06%
F3	-0.18%	-0.02%	0.07%
F4	-0.21%	0.03%	0.14%
C1	0.35%	0.08%	-0.03%
C2	0.28%	0.20%	0.17%
RR	0.23%	-0.18%	-0.23%
PR	-0.16%	-0.07%	-0.06%

Table 10: Region-dependent percentage difference between 'thermal group' average fluxes from homogenized diffusion (FDM) and transport (VARIANT) results for ARI HTTR configuration.

These difference across the permanent reflector region, however, do not significantly impact the fundamental eigenvalue (and hence eigenmode) of the core. In fact, the difference between the homogenized diffusion and homogenized transport eigenvalues is well below one hundred percent mille.

The suitability (and accuracy) of the simple homogenization procedure has been established with respect to fine-mesh heterogeneous transport. In addition, a comparison has been performed in order to assess the differences between the diffusion and transport solutions at the homogenized core level. While the use of diffusion over coarse homogenized cell is acceptable (with respect to a reference nodal transport solution), the flux-weighted homogenization is not sufficient to capture the correct absorption due to the CR blocks inserted into the core. Nonetheless, the macroscopic cross-section data and results obtained thus far are sufficient to perform a comparison between certain diffusion solvers. The 'homogenized' core representation not only simplified the actual heterogeneous problem, but allows the use of fast and accurate nodal diffusion methods. In this particular work, we compare two nodal diffusion methodologies: the Nodal Expansion Method (NEM) and the Nodal Green's Function Method (NGFM).

III.B. Nodal Diffusion Methods

In this section we compare two standard implementations of nodal diffusion methods to the fine-mesh FDM results presented in the previous sub-section. In particular, the HEXPEDITE [17] [18] [19] implementation of the NGFM approach will be compared alongside with the NEM implemented into the DIF3D code system. A comparison of the eigenvalue results for all three HTTR configurations between the NGFM and NEM results is shown in Tables 11 through 13.

Code	Method	k-eff
HEXPEDITE	NGFM	0.88787
	Error (pcm)	-17.0
DIF3D	NEM	0.88050
	Error (pcm)	-847.3
DIF3D	Fine Mesh FD	0.88802

Table 11: Comparison of NGFM and NEM eigenvalue results to fine-mesh FDM for ARI HTTR configuration.

Code	Method	k-eff
HEXPEDITE	NGFM	1.00198
	Error (pcm)	-186.9
DIF3D	NEM	0.99904
	Error (pcm)	-479.1
DIF3D	Fine Mesh FD	1.00385

Table 12: Comparison of NGFM and NEM eigenvalue results to fine-mesh FDM for PI HTTR configuration.

Code	Method	k-eff
HEXPEDITE	NGFM	1.09811
	Error (pcm)	12.3
DIF3D	NEM	1.09348
	Error (pcm)	-409.1
DIF3D	Fine Mesh FD	1.09798

Table 13: Comparison of NGFM and NEM eigenvalue results to fine-mesh FDM for ARO HTTR configuration.

In summary, the NGFM results agree rather well with the FDM results in all three cases. The ARI and ARO configurations show a particularly good agreement between the two methodologies. However, the NEM results show significant disagreement with respect to the FDM results, especially in the ARI configuration. A comparison of the normalized fission distribution reveals that the maximum error between NGFM and FDM is -0.72 %, whereas the maximum error between NEM and FDM is 1.62 %. In addition, the error in the

normalized absorption across the CR blocks between the NGFM and FDM is -0.06 %, whereas the error between the NEM and FDM for the normalized absorption rate is 2.82 %. A comparison of analogous quantities for the other two HTTR configurations reveals a similar trend, in which the NGFM solution is closer to the FDM than the NEM results.

IV. CONCLUSION

This work has focused on two main tasks; the solution of the Simplified HTTR Numerical Benchmark via the deterministic transport methods, in particular the Collision Probability (CP) and Method of Characteristic (MOC) solver options available in HELIOS, and the generation of flux-weighted homogenized data for all three HTTR configurations (All Rods Inserted, Partially Inserted, and All Rods Out). The MOC option was selected after numerous comparisons to the reference multi-group Monte Carlo results and used to spatially homogenize the cross-sections without any form of energy condensation.

Once these data were prepared, a fine-mesh Finite Difference Method (FDM) solver for the diffusion equation was used to obtain a 'reference' diffusion solution. In addition, the nodal transport solver VARIANT was used to generate a 'reference' transport solution for the homogenized reactor problem. The numerical results show that large error are incurred by 'naively' homogenizing CR blocks by simple flux-weighted homogenization in both FDM diffusion and VARIANT solutions (with respect to the reference heterogeneous MOC solution). In addition, a comparison between the diffusion and transport solution for the homogenized model revealed significant differences in the flux solution at the periphery of the domain (across permanent reflector region) for the fast-energy groups. However, these differences do not have a significant impact on the core eigenvalue results, as evidenced by the close agreement between the fine-mesh FDM diffusion theory and nodal transport results.

Finally, a comparison between two nodal diffusion solvers was performed and compared to the fine-mesh FDM solution. Namely, the Nodal Expansion Method (NEM) and the Nodal Green's Function Method (NGFM) were compared against the fine-mesh FDM solution in order to determine the adequacy of the solution. Results show that the NGFM method is more accurate than the NEM approach with respect to the fine-mesh FDM. This is expected, since the NEM implementation in DIF3D is geared towards fast reactor analysis (in which the flux does not undergo any large gradients), whereas the HEXPEDITE implementation of the NGFM approach has been tested and shown to be very accurate for a wide variety of reactor types. Finally, the set of homogenized macroscopic cross-section for diffusion solvers is included in this article.

Recommendations for future work include a systematic study of the spatial homogenization procedure in order to quantify the error between cross-section generated from a 'lattice' HELIOS calculation and the reference full-core solution, since it is not practical to use the full-core model for routine production calculations. In addition, the development and implementation of an advanced treatment for the control-rod regions into either a diffusion theory or transport solver at the homogenized level is necessary in order to improve the accuracy the eigenvalue estimates for the 'All Rods Inserted' HTTR configuration. Finally, the addition of anisotropic scattering to the VARIANT results could further clarify the differences between the diffusion and transport theory results for the homogeneous model of the HTTR core. Since this is a two-dimensional benchmark, there may be yet-unaccounted-for effects in three-dimensional configurations. Hence, it would be valuable to perform this study at the three-dimensional level. However, this further complicates the generation of cross-section until the 'lattice' approach is validated.

V. ACKNOWLEDGEMENTS

This work is supported by the U.S. Department of Energy, Assistant Secretary for the office of Nuclear Energy, under DOE Idaho Operations Office Contract DEA07-05ID14517.

The first author would like to acknowledge Charles Wemple (Studsvik Scandpower) for his help in the generation of HELIOS cross-section libraries and comments regarding correct modeling procedures.

REFERENCES

[1] E. Wachspress, *Iterative Solution of Elliptic Systems and Applications to the Neutron Diffusion Equations of Reactor Physics*, Prentice-Hall, 1966.

[2] R. D. Lawrence, "Progress in Nodal Methods for the Solution of the Neutron Diffusion and Transport Equations," *Prog. Nucl. Eng.*, Vol. 17, No. 3, pp. 271-301, 1986.

[3] J. W. Sterbentz, B. Phillips, R. L. Sant, G.S. Chang, and P. D. Bayless, "Reactor Physics Parametric and Depletion Studies in Support of TRISO Particle Fuel Specification for the Next Generation Nuclear Plant," INEEL/EXT-04-02331, September 2004.

[4] A. M. Ougouag, "Systematics of Neutron Diffusion Modeling for Neutron-Optically Thin, Multiply-Heterogeneous High Temperature Reactors," INL/EXT-09-16414, July 2009.

[5] "Argonne Code Center: Benchmark Book," ANL-7416, Argonne National Laboratory, December 1985.

[6] Z. Zhang, F. Rahnema, J. M. Pounders, D. Zhang, and A. M. Ougouag, "A Simplified 2D HTTR Benchmark Problem," Proc. of the Int.

Topl. Meeting on Mathematics, Computational Methods, & Reactor Physics (M&C 2009), Saratoga Springs, New York, May 3-7, 2009.

[7] N. Nojiri, N. Nakano, et al., "Benchmark Problem's Data for HTTR's Start-up Core Physics Experiments," JAERI-memo 10-1005, Japan, 1998.

[8] X. Raepsaet, et al., "Analysis of the European Results on the HTTR's Core Physics Benchmarks," *Nuclear Engineering and Design,* 222, pp. 173-187, 2003.

[9] C. A. Wemple, H-N. M. Gheorghiu, R. J. J. Stamm'ler, and E. A. Villarino, "Recent Advances in the HELIOS-2 Lattice Physics Code," Int. Conf. on Physics of Reactors (PHYSOR 2008), Interlaken, Switzerland, September 14-19, 2008.

[10] X-5 Monte Carlo Team, "MCNP – A General Monte Carlo N-Particle Transport Code, Version 5", Los Alamos National Laboratory, LA-CP-03-0245, 2003.

[11] J. M Pounders, F. Rahnema, "On the Diffusion Coefficients for Reactor Physics Applications," *Nucl. Sci. Eng.,* Vol. 163, 3, November 2009.

[12] S. Mosher, F. Rahnema, "The Incident Flux Response Expansion Method for Heterogeneous Coarse Mesh Transport Problems," *Transport Theory and Statistical Physics,* 34, pp. 1-26, 2006.

[13] K. S. Smith, Assembly homogenization techniques for light water reactors. *Prog. Nucl. Energy* 17, 303, 1986.

[14] R. Sanchez, Assembly Homogenization Techniques for Core Calculations. *Prog. Nucl. Energy* 51, 14-31, 2009.

[15] R. D. Lawrence, The DIF3D Nodal Neutronics Option for Two- and Three-Dimensional Diffusion Theory Calculations in Hexagonal Geometry, Argonne National Laboratory, ANL-83-1, March 1983.

[16] G. Pamiotti, E. E. Lewis, and C. B. Carrico, "VARIANT: VARIational Anisotropic Nodal Transport," ANL-95/40, October 1995.

[17] W. E. Fitzpatrick and A. M. Ougouag, "HEXPEDITE: A Net Current Multigroup Nodal Diffusion Method for Hexagonal-z Geometry," *Trans. Am. Nucl. Soc.,* Vol. 66, 1992.

[18] A. M. Ougouag and W. Fitzpatrick, "An Inherently Parallel Multigroup Nodal Diffusion Method for Hexagonal-Z Geometry," *Fourth International Conference on Simulation Methods in Nuclear Engineering*, Montreal, Canada, June 2-4, 1993.

[19] W. E. Fitzpatrick, *Developments in Nodal Reactor Analysis Tools for Hexagonal Geometry,* Doctoral dissertation, University of Illinois at Urbana-Champaign, 1995.

V. APPENDIX: CROSS-SECTION DATA

V.A. Case 1: All Rods Inserted

Material 1: Fuel Block Type 1

group	diffusion	removal	nu fission	fission	chi
1	1.77327E+00	1.41950E-02	1.69172E-04	6.21808E-05	9.69182E-01
2	1.02215E+00	1.02280E-02	9.75332E-05	4.00962E-05	3.08180E-02
3	9.75752E-01	9.54202E-03	8.06291E-04	3.31289E-04	0.00000E+00
4	9.86634E-01	5.19500E-02	1.19386E-03	4.90534E-04	0.00000E+00
5	9.64877E-01	4.44420E-02	4.68363E-03	1.92442E-03	0.00000E+00
6	8.89501E-01	9.95380E-02	1.01146E-02	4.15589E-03	0.00000E+00

Scattering	matrix					
1	0.00000E+00	0.00000E+00	0.00000E+00	0.00000E+00	0.00000E+00	0.00000E+00
2	1.41020E-02	0.00000E+00	0.00000E+00	0.00000E+00	0.00000E+00	0.00000E+00
3	0.00000E+00	9.98725E-03	0.00000E+00	1.02285E-04	0.00000E+00	0.00000E+00
4	0.00000E+00	0.00000E+00	6.56138E-03	0.00000E+00	4.13372E-03	3.52192E-07
5	0.00000E+00	0.00000E+00	0.00000E+00	5.07046E-02	0.00000E+00	9.27961E-02
6	0.00000E+00	0.00000E+00	0.00000E+00	2.44399E-06	3.69830E-02	0.00000E+00

Material 2: Fuel Block Type 2

group	diffusion	removal	nu fission	fission	chi
1	1.77533E+00	1.41760E-02	1.75508E-04	6.46753E-05	9.69182E-01
2	1.02302E+00	1.02190E-02	1.14251E-04	4.69695E-05	3.08180E-02
3	9.76137E-01	9.59000E-03	9.40721E-04	3.86522E-04	0.00000E+00
4	9.86967E-01	5.18220E-02	1.39306E-03	5.72382E-04	0.00000E+00
5	9.63611E-01	4.46540E-02	5.40360E-03	2.22023E-03	0.00000E+00
6	8.86813E-01	1.00455E-01	1.16408E-02	4.78298E-03	0.00000E+00

Scattering	matrix					
1	0.00000E+00	0.00000E+00	0.00000E+00	0.00000E+00	0.00000E+00	0.00000E+00
2	1.40811E-02	0.00000E+00	0.00000E+00	0.00000E+00	0.00000E+00	0.00000E+00
3	0.00000E+00	9.96976E-03	0.00000E+00	1.02643E-04	0.00000E+00	0.00000E+00
4	0.00000E+00	0.00000E+00	6.53687E-03	0.00000E+00	4.21347E-03	3.51860E-07
5	0.00000E+00	0.00000E+00	0.00000E+00	5.04752E-02	0.00000E+00	9.29768E-02
6	0.00000E+00	0.00000E+00	0.00000E+00	2.42464E-06	3.67648E-02	0.00000E+00

Material 3: Fuel Block Type 3

group	diffusion	removal	nu fission	fission	chi
1	1.77971E+00	1.41380E-02	1.83212E-04	6.76910E-05	9.69182E-01
2	1.02463E+00	1.02020E-02	1.32982E-04	5.46699E-05	3.08180E-02
3	9.76772E-01	9.64800E-03	1.08807E-03	4.47069E-04	0.00000E+00
4	9.87409E-01	5.17190E-02	1.61023E-03	6.61615E-04	0.00000E+00
5	9.61496E-01	4.49160E-02	6.13707E-03	2.52160E-03	0.00000E+00
6	8.82373E-01	1.01532E-01	1.30836E-02	5.37580E-03	0.00000E+00

Scattering	matrix					
1	0.00000E+00	0.00000E+00	0.00000E+00	0.00000E+00	0.00000E+00	0.00000E+00
2	1.40398E-02	0.00000E+00	0.00000E+00	0.00000E+00	0.00000E+00	0.00000E+00
3	0.00000E+00	9.94472E-03	0.00000E+00	1.02918E-04	0.00000E+00	0.00000E+00
4	0.00000E+00	0.00000E+00	6.51050E-03	0.00000E+00	4.29623E-03	3.50491E-07
5	0.00000E+00	0.00000E+00	0.00000E+00	5.02626E-02	0.00000E+00	9.33568E-02
6	0.00000E+00	0.00000E+00	0.00000E+00	2.40800E-06	3.65848E-02	0.00000E+00

Material 4: Fuel Block Type 4

group	diffusion	removal	nu fission	fission	chi
1	1.78431E+00	1.41000E-02	1.91180E-04	7.07318E-05	9.69182E-01
2	1.02584E+00	1.01920E-02	1.45830E-04	5.99520E-05	3.08180E-02
3	9.76738E-01	9.70203E-03	1.18398E-03	4.86473E-04	0.00000E+00
4	9.87186E-01	5.16940E-02	1.75082E-03	7.19378E-04	0.00000E+00
5	9.59343E-01	4.51180E-02	6.58239E-03	2.70456E-03	0.00000E+00
6	8.78543E-01	1.02287E-01	1.38956E-02	5.70946E-03	0.00000E+00

Scattering	matrix					
1	0.00000E+00	0.00000E+00	0.00000E+00	0.00000E+00	0.00000E+00	0.00000E+00
2	1.39977E-02	0.00000E+00	0.00000E+00	0.00000E+00	0.00000E+00	0.00000E+00
3	0.00000E+00	9.92568E-03	0.00000E+00	1.03318E-04	0.00000E+00	0.00000E+00
4	0.00000E+00	0.00000E+00	6.49413E-03	0.00000E+00	4.34922E-03	3.49361E-07

5	0.00000E+00	0.00000E+00	0.00000E+00	5.01651E-02	0.00000E+00	9.37147E-02
6	0.00000E+00	0.00000E+00	0.00000E+00	2.40014E-06	3.65121E-02	0.00000E+00

Material 5: Control Rod Block

group	diffusion	removal
1	1.57418E+00	1.83670E-02
2	9.50187E-01	1.23670E-02
3	9.29020E-01	9.61900E-03
4	9.15912E-01	5.31370E-02
5	8.86268E-01	5.38860E-02
6	8.23938E-01	8.19570E-02

Scattering	matrix					
1	0.00000E+00	0.00000E+00	0.00000E+00	0.00000E+00	0.00000E+00	0.00000E+00
2	1.83660E-02	0.00000E+00	0.00000E+00	0.00000E+00	0.00000E+00	0.00000E+00
3	0.00000E+00	1.23502E-02	0.00000E+00	3.72980E-05	0.00000E+00	0.00000E+00
4	0.00000E+00	0.00000E+00	9.32977E-03	0.00000E+00	2.14365E-03	0.00000E+00
5	0.00000E+00	0.00000E+00	0.00000E+00	5.19090E-02	0.00000E+00	7.83177E-02
6	0.00000E+00	0.00000E+00	0.00000E+00	7.60525E-07	4.95049E-02	0.00000E+00

Material 6: Removable Reflector

group	diffusion	removal
1	1.44636E+00	1.99920E-02
2	8.63406E-01	1.34690E-02
3	8.39559E-01	1.04020E-02
4	8.38414E-01	5.77590E-02
5	8.27670E-01	5.80830E-02
6	7.80569E-01	8.28590E-02

Scattering	matrix					
1	0.00000E+00	0.00000E+00	0.00000E+00	0.00000E+00	0.00000E+00	0.00000E+00
2	1.99918E-02	0.00000E+00	0.00000E+00	0.00000E+00	0.00000E+00	0.00000E+00
3	0.00000E+00	1.34684E-02	0.00000E+00	4.00764E-05	0.00000E+00	0.00000E+00
4	0.00000E+00	0.00000E+00	1.03913E-02	0.00000E+00	1.91158E-03	0.00000E+00
5	0.00000E+00	0.00000E+00	0.00000E+00	5.76691E-02	0.00000E+00	8.26249E-02
6	0.00000E+00	0.00000E+00	0.00000E+00	8.53909E-07	5.60562E-02	0.00000E+00

Material 7: Permanent Reflector

group	diffusion	removal
1	1.48853E+00	1.94030E-02
2	8.88375E-01	1.30730E-02
3	8.63732E-01	1.00930E-02
4	8.62811E-01	5.61150E-02
5	8.51707E-01	5.63340E-02
6	8.03203E-01	8.06320E-02

Scattering	matrix					
1	0.00000E+00	0.00000E+00	0.00000E+00	0.00000E+00	0.00000E+00	0.00000E+00
2	1.94024E-02	0.00000E+00	0.00000E+00	0.00000E+00	0.00000E+00	0.00000E+00
3	0.00000E+00	1.30717E-02	0.00000E+00	3.89547E-05	0.00000E+00	0.00000E+00
4	0.00000E+00	0.00000E+00	1.00794E-02	0.00000E+00	1.87790E-03	0.00000E+00
5	0.00000E+00	0.00000E+00	0.00000E+00	5.60121E-02	0.00000E+00	8.03264E-02
6	0.00000E+00	0.00000E+00	0.00000E+00	8.29065E-07	5.43056E-02	0.00000E+00

V.B. Case 2: Partially Inserted

Material 1: Fuel Block Type 1

group	diffusion	removal	nu fission	fission	chi
1	1.77280E+00	1.41990E-02	1.68929E-04	6.20913E-05	9.69182E-01
2	1.02198E+00	1.02300E-02	9.74430E-05	4.00591E-05	3.08180E-02
3	9.75649E-01	9.53999E-03	8.05741E-04	3.31063E-04	0.00000E+00
4	9.86438E-01	5.19600E-02	1.19252E-03	4.89984E-04	0.00000E+00
5	9.64208E-01	4.44650E-02	4.66414E-03	1.91641E-03	0.00000E+00
6	8.88756E-01	9.95980E-02	1.00605E-02	4.13365E-03	0.00000E+00

Scattering	matrix					
1	0.00000E+00	0.00000E+00	0.00000E+00	0.00000E+00	0.00000E+00	0.00000E+00
2	1.41062E-02	0.00000E+00	0.00000E+00	0.00000E+00	0.00000E+00	0.00000E+00
3	0.00000E+00	9.98903E-03	0.00000E+00	1.02276E-04	0.00000E+00	0.00000E+00
4	0.00000E+00	0.00000E+00	6.56219E-03	0.00000E+00	4.13650E-03	3.51639E-07
5	0.00000E+00	0.00000E+00	0.00000E+00	5.07153E-02	0.00000E+00	9.28804E-02
6	0.00000E+00	0.00000E+00	0.00000E+00	2.44422E-06	3.70112E-02	0.00000E+00

Material 2: Fuel Block Type 2

group	diffusion	removal	nu fission	fission	chi
1	1.77602E+00	1.41710E-02	1.75872E-04	6.48094E-05	9.69182E-01
2	1.02327E+00	1.02160E-02	1.14413E-04	4.70359E-05	3.08180E-02
3	9.76229E-01	9.59200E-03	9.41305E-04	3.86762E-04	0.00000E+00
4	9.86888E-01	5.18250E-02	1.39246E-03	5.72137E-04	0.00000E+00
5	9.62618E-01	4.46870E-02	5.37008E-03	2.20646E-03	0.00000E+00
6	8.85613E-01	1.00547E-01	1.15377E-02	4.74060E-03	0.00000E+00

Scattering	matrix					
1	0.00000E+00	0.00000E+00	0.00000E+00	0.00000E+00	0.00000E+00	0.00000E+00
2	1.40751E-02	0.00000E+00	0.00000E+00	0.00000E+00	0.00000E+00	0.00000E+00
3	0.00000E+00	9.96704E-03	0.00000E+00	1.02640E-04	0.00000E+00	0.00000E+00
4	0.00000E+00	0.00000E+00	6.53614E-03	0.00000E+00	4.21714E-03	3.50947E-07
5	0.00000E+00	0.00000E+00	0.00000E+00	5.04795E-02	0.00000E+00	9.31147E-02
6	0.00000E+00	0.00000E+00	0.00000E+00	2.42474E-06	3.68083E-02	0.00000E+00

Material 3: Fuel Block Type 3

group	diffusion	removal	nu fission	fission	chi

1	1.77932E+00	1.41410E-02	1.82996E-04	6.76110E-05	9.69182E-01
2	1.02449E+00	1.02030E-02	1.32878E-04	5.46268E-05	3.08180E-02
3	9.76672E-01	9.64698E-03	1.08734E-03	4.46767E-04	0.00000E+00
4	9.87221E-01	5.17290E-02	1.60847E-03	6.60891E-04	0.00000E+00
5	9.60775E-01	4.49400E-02	6.10898E-03	2.51006E-03	0.00000E+00
6	8.81657E-01	1.01583E-01	1.30115E-02	5.34620E-03	0.00000E+00

Scattering	matrix					
1	0.00000E+00	0.00000E+00	0.00000E+00	0.00000E+00	0.00000E+00	0.00000E+00
2	1.40433E-02	0.00000E+00	0.00000E+00	0.00000E+00	0.00000E+00	0.00000E+00
3	0.00000E+00	9.94622E-03	0.00000E+00	1.02908E-04	0.00000E+00	0.00000E+00
4	0.00000E+00	0.00000E+00	6.51131E-03	0.00000E+00	4.29855E-03	3.49932E-07
5	0.00000E+00	0.00000E+00	0.00000E+00	5.02732E-02	0.00000E+00	9.34405E-02
6	0.00000E+00	0.00000E+00	0.00000E+00	2.40824E-06	3.66177E-02	0.00000E+00

Material 4: Fuel Block Type 4

group	diffusion	removal	nu fission	fission	chi
1	1.78391E+00	1.41030E-02	1.90965E-04	7.06523E-05	9.69182E-01
2	1.02570E+00	1.01940E-02	1.45715E-04	5.99047E-05	3.08180E-02
3	9.76615E-01	9.70000E-03	1.18305E-03	4.86093E-04	0.00000E+00
4	9.87014E-01	5.17030E-02	1.74907E-03	7.18656E-04	0.00000E+00
5	9.58697E-01	4.51390E-02	6.55486E-03	2.69325E-03	0.00000E+00
6	8.77962E-01	1.02326E-01	1.38306E-02	5.68276E-03	0.00000E+00

Scattering	matrix					
1	0.00000E+00	0.00000E+00	0.00000E+00	0.00000E+00	0.00000E+00	0.00000E+00
2	1.40011E-02	0.00000E+00	0.00000E+00	0.00000E+00	0.00000E+00	0.00000E+00
3	0.00000E+00	9.92723E-03	0.00000E+00	1.03308E-04	0.00000E+00	0.00000E+00
4	0.00000E+00	0.00000E+00	6.49514E-03	0.00000E+00	4.35112E-03	3.48890E-07
5	0.00000E+00	0.00000E+00	0.00000E+00	5.01752E-02	0.00000E+00	9.37833E-02
6	0.00000E+00	0.00000E+00	0.00000E+00	2.40038E-06	3.65426E-02	0.00000E+00

Material 5: Withdrawn Control Rod Block

group	diffusion	removal
1	1.51719E+00	1.90580E-02
2	9.25903E-01	1.26800E-02
3	9.06585E-01	9.58198E-03
4	9.14982E-01	5.22240E-02
5	9.34071E-01	4.93960E-02
6	8.85917E-01	7.36740E-02

Scattering	matrix					
1	0.00000E+00	0.00000E+00	0.00000E+00	0.00000E+00	0.00000E+00	0.00000E+00
2	1.90578E-02	0.00000E+00	0.00000E+00	0.00000E+00	0.00000E+00	0.00000E+00

3	0.00000E+00	1.26797E-02	0.00000E+00	3.70093E-05	0.00000E+00	0.00000E+00
4	0.00000E+00	0.00000E+00	9.57207E-03	0.00000E+00	2.04567E-03	0.00000E+00
5	0.00000E+00	0.00000E+00	0.00000E+00	5.21421E-02	0.00000E+00	7.34687E-02
6	0.00000E+00	0.00000E+00	0.00000E+00	7.64326E-07	4.72492E-02	0.00000E+00

Material 6: Control Rod Block

group	diffusion	removal
1	1.57412E+00	1.83690E-02
2	9.49546E-01	1.23750E-02
3	9.27936E-01	9.62701E-03
4	9.14241E-01	5.32130E-02
5	8.84692E-01	5.39330E-02
6	8.22237E-01	8.20180E-02

Scattering	matrix					
1	0.00000E+00	0.00000E+00	0.00000E+00	0.00000E+00	0.00000E+00	0.00000E+00
2	1.83666E-02	0.00000E+00	0.00000E+00	0.00000E+00	0.00000E+00	0.00000E+00
3	0.00000E+00	1.23586E-02	0.00000E+00	3.73591E-05	0.00000E+00	0.00000E+00
4	0.00000E+00	0.00000E+00	9.34079E-03	0.00000E+00	2.14781E-03	0.00000E+00
5	0.00000E+00	0.00000E+00	0.00000E+00	5.20077E-02	0.00000E+00	7.85066E-02
6	0.00000E+00	0.00000E+00	0.00000E+00	7.61980E-07	4.96010E-02	0.00000E+00

Material 7: Removable Reflector

group	diffusion	removal
1	1.44636E+00	1.99920E-02
2	8.63406E-01	1.34690E-02
3	8.39561E-01	1.04020E-02
4	8.38418E-01	5.77580E-02
5	8.27666E-01	5.80830E-02
6	7.80569E-01	8.28590E-02

Scattering	matrix					
1	0.00000E+00	0.00000E+00	0.00000E+00	0.00000E+00	0.00000E+00	0.00000E+00
2	1.99918E-02	0.00000E+00	0.00000E+00	0.00000E+00	0.00000E+00	0.00000E+00
3	0.00000E+00	1.34684E-02	0.00000E+00	4.00762E-05	0.00000E+00	0.00000E+00
4	0.00000E+00	0.00000E+00	1.03913E-02	0.00000E+00	1.91158E-03	0.00000E+00
5	0.00000E+00	0.00000E+00	0.00000E+00	5.76689E-02	0.00000E+00	8.26247E-02
6	0.00000E+00	0.00000E+00	0.00000E+00	8.53905E-07	5.60564E-02	0.00000E+00

Material 8: Permanent Reflector

group	diffusion	removal
1	1.48851E+00	1.94030E-02
2	8.88358E-01	1.30730E-02
3	8.63708E-01	1.00940E-02
4	8.62814E-01	5.61150E-02

5	8.51707E-01	5.63340E-02
6	8.03203E-01	8.06320E-02

Scattering	matrix					
1	0.00000E+00	0.00000E+00	0.00000E+00	0.00000E+00	0.00000E+00	0.00000E+00
2	1.94027E-02	0.00000E+00	0.00000E+00	0.00000E+00	0.00000E+00	0.00000E+00
3	0.00000E+00	1.30720E-02	0.00000E+00	3.89547E-05	0.00000E+00	0.00000E+00
4	0.00000E+00	0.00000E+00	1.00797E-02	0.00000E+00	1.87790E-03	0.00000E+00
5	0.00000E+00	0.00000E+00	0.00000E+00	5.60121E-02	0.00000E+00	8.03265E-02
6	0.00000E+00	0.00000E+00	0.00000E+00	8.29064E-07	5.43056E-02	0.00000E+00

V.C. Case 3: All Rods Out

Material 1: Fuel Block Type 1

group	diffusion	removal	nu fission	fission	chi
1	1.77307E+00	1.41960E-02	1.69070E-04	6.21431E-05	9.69182E-01
2	1.02205E+00	1.02290E-02	9.74816E-05	4.00750E-05	3.08180E-02
3	9.75637E-01	9.54002E-03	8.05675E-04	3.31036E-04	0.00000E+00
4	9.86348E-01	5.19650E-02	1.19187E-03	4.89719E-04	0.00000E+00
5	9.63678E-01	4.44840E-02	4.64876E-03	1.91009E-03	0.00000E+00
6	8.88119E-01	9.96500E-02	1.00142E-02	4.11465E-03	0.00000E+00

Scattering	matrix					
1	0.00000E+00	0.00000E+00	0.00000E+00	0.00000E+00	0.00000E+00	0.00000E+00
2	1.41037E-02	0.00000E+00	0.00000E+00	0.00000E+00	0.00000E+00	0.00000E+00
3	0.00000E+00	9.98828E-03	0.00000E+00	1.02271E-04	0.00000E+00	0.00000E+00
4	0.00000E+00	0.00000E+00	6.56227E-03	0.00000E+00	4.13870E-03	3.51167E-07
5	0.00000E+00	0.00000E+00	0.00000E+00	5.07203E-02	0.00000E+00	9.29525E-02
6	0.00000E+00	0.00000E+00	0.00000E+00	2.44432E-06	3.70336E-02	0.00000E+00

Material 2: Fuel Block Type 2

group	diffusion	removal	nu fission	fission	chi
1	1.77494E+00	1.41800E-02	1.75304E-04	6.46001E-05	9.69182E-01
2	1.02287E+00	1.02200E-02	1.14153E-04	4.69289E-05	3.08180E-02
3	9.76000E-01	9.58899E-03	9.39877E-04	3.86175E-04	0.00000E+00
4	9.86660E-01	5.18380E-02	1.39062E-03	5.71382E-04	0.00000E+00
5	9.62340E-01	4.46970E-02	5.36071E-03	2.20261E-03	0.00000E+00
6	8.85378E-01	1.00565E-01	1.15180E-02	4.73252E-03	0.00000E+00

Scattering	matrix					
1	0.00000E+00	0.00000E+00	0.00000E+00	0.00000E+00	0.00000E+00	0.00000E+00
2	1.40845E-02	0.00000E+00	0.00000E+00	0.00000E+00	0.00000E+00	0.00000E+00
3	0.00000E+00	9.97140E-03	0.00000E+00	1.02628E-04	0.00000E+00	0.00000E+00
4	0.00000E+00	0.00000E+00	6.53797E-03	0.00000E+00	4.21816E-03	3.50774E-07

5	0.00000E+00	0.00000E+00	0.00000E+00	5.04922E-02	0.00000E+00	9.31414E-02
6	0.00000E+00	0.00000E+00	0.00000E+00	2.42502E-06	3.68205E-02	0.00000E+00

Material 3: Fuel Block Type 3

group	diffusion	removal	nu fission	fission	chi
1	1.77983E+00	1.41380E-02	1.83273E-04	6.77134E-05	9.69182E-01
2	1.02467E+00	1.02020E-02	1.33008E-04	5.46803E-05	3.08180E-02
3	9.76758E-01	9.64803E-03	1.08795E-03	4.47019E-04	0.00000E+00
4	9.87253E-01	5.17270E-02	1.60879E-03	6.61024E-04	0.00000E+00
5	9.60133E-01	4.49610E-02	6.08392E-03	2.49976E-03	0.00000E+00
6	8.80851E-01	1.01641E-01	1.29302E-02	5.31280E-03	0.00000E+00

Scattering	matrix					
1	0.00000E+00	0.00000E+00	0.00000E+00	0.00000E+00	0.00000E+00	0.00000E+00
2	1.40388E-02	0.00000E+00	0.00000E+00	0.00000E+00	0.00000E+00	0.00000E+00
3	0.00000E+00	9.94433E-03	0.00000E+00	1.02910E-04	0.00000E+00	0.00000E+00
4	0.00000E+00	0.00000E+00	6.51062E-03	0.00000E+00	4.30062E-03	3.49301E-07
5	0.00000E+00	0.00000E+00	0.00000E+00	5.02715E-02	0.00000E+00	9.35350E-02
6	0.00000E+00	0.00000E+00	0.00000E+00	2.40821E-06	3.66471E-02	0.00000E+00

Material 4: Fuel Block Type 4

group	diffusion	removal	nu fission	fission	chi
1	1.78465E+00	1.40970E-02	1.91372E-04	7.08026E-05	9.69182E-01
2	1.02601E+00	1.01910E-02	1.45965E-04	6.00076E-05	3.08180E-02
3	9.76827E-01	9.70298E-03	1.18466E-03	4.86754E-04	0.00000E+00
4	9.87186E-01	5.16940E-02	1.75080E-03	7.19370E-04	0.00000E+00
5	9.58061E-01	4.51600E-02	6.52755E-03	2.68203E-03	0.00000E+00
6	8.77161E-01	1.02381E-01	1.37418E-02	5.64627E-03	0.00000E+00

Scattering	matrix					
1	0.00000E+00	0.00000E+00	0.00000E+00	0.00000E+00	0.00000E+00	0.00000E+00
2	1.39947E-02	0.00000E+00	0.00000E+00	0.00000E+00	0.00000E+00	0.00000E+00
3	0.00000E+00	9.92383E-03	0.00000E+00	1.03317E-04	0.00000E+00	0.00000E+00
4	0.00000E+00	0.00000E+00	6.49342E-03	0.00000E+00	4.35298E-03	3.48249E-07
5	0.00000E+00	0.00000E+00	0.00000E+00	5.01652E-02	0.00000E+00	9.38786E-02
6	0.00000E+00	0.00000E+00	0.00000E+00	2.40014E-06	3.65726E-02	0.00000E+00

Material 5: Control Rod Block

group	diffusion	removal
1	1.52235E+00	1.89940E-02
2	9.51530E-01	1.23390E-02
3	9.34953E-01	9.29201E-03
4	9.37633E-01	5.09630E-02
5	9.30867E-01	4.95660E-02
6	8.80451E-01	7.41320E-02

Scattering	matrix					
1	0.00000E+00	0.00000E+00	0.00000E+00	0.00000E+00	0.00000E+00	0.00000E+00
2	1.89932E-02	0.00000E+00	0.00000E+00	0.00000E+00	0.00000E+00	0.00000E+00
3	0.00000E+00	1.23382E-02	0.00000E+00	3.61152E-05	0.00000E+00	0.00000E+00
4	0.00000E+00	0.00000E+00	9.28164E-03	0.00000E+00	2.05271E-03	0.00000E+00
5	0.00000E+00	0.00000E+00	0.00000E+00	5.08825E-02	0.00000E+00	7.39248E-02
6	0.00000E+00	0.00000E+00	0.00000E+00	7.45861E-07	4.74118E-02	0.00000E+00

Material 6: Removable Reflector

group	diffusion	removal
1	1.44636E+00	1.99920E-02
2	8.63406E-01	1.34690E-02
3	8.39557E-01	1.04020E-02
4	8.38420E-01	5.77580E-02
5	8.27668E-01	5.80830E-02
6	7.80571E-01	8.28590E-02

Scattering	matrix					
1	0.00000E+00	0.00000E+00	0.00000E+00	0.00000E+00	0.00000E+00	0.00000E+00
2	1.99918E-02	0.00000E+00	0.00000E+00	0.00000E+00	0.00000E+00	0.00000E+00
3	0.00000E+00	1.34684E-02	0.00000E+00	4.00761E-05	0.00000E+00	0.00000E+00
4	0.00000E+00	0.00000E+00	1.03913E-02	0.00000E+00	1.91158E-03	0.00000E+00
5	0.00000E+00	0.00000E+00	0.00000E+00	5.76688E-02	0.00000E+00	8.26246E-02
6	0.00000E+00	0.00000E+00	0.00000E+00	8.53904E-07	5.60564E-02	0.00000E+00

Material 7: Permanent Reflector

group	diffusion	removal
1	1.48853E+00	1.94030E-02
2	8.88372E-01	1.30730E-02
3	8.63739E-01	1.00930E-02
4	8.62822E-01	5.61140E-02
5	8.51722E-01	5.63330E-02
6	8.03188E-01	8.06340E-02

Scattering	matrix					
1	0.00000E+00	0.00000E+00	0.00000E+00	0.00000E+00	0.00000E+00	0.00000E+00
2	1.94024E-02	0.00000E+00	0.00000E+00	0.00000E+00	0.00000E+00	0.00000E+00
3	0.00000E+00	1.30717E-02	0.00000E+00	3.89542E-05	0.00000E+00	0.00000E+00
4	0.00000E+00	0.00000E+00	1.00793E-02	0.00000E+00	1.87787E-03	0.00000E+00
5	0.00000E+00	0.00000E+00	0.00000E+00	5.60114E-02	0.00000E+00	8.03279E-02
6	0.00000E+00	0.00000E+00	0.00000E+00	8.29054E-07	5.43046E-02	0.00000E+00